Probing alloy composition gradient and nanometer-scale carrier localization in single AlGaN nanowires by nanocathodoluminescence

2013 Nanotechnology 24 305703

(http://iopscience.iop.org/0957-4484/24/30/305703)

Nanotechnology **24** (2013) 305703 (7pp) doi:10.1088/0957-4484/24/30/305703

Probing alloy composition gradient and nanometer-scale carrier localization in single AlGaN nanowires by nanocathodoluminescence

A Pierret[1,2], C Bougerol[3], B Gayral[1], M Kociak[4] and B Daudin[1]

[1] CEA-CNRS group 'Nanophysique et Semiconducteurs', Institut Néel/CNRS-Université J Fourier and CEA Grenoble, INAC, SP2M, 17 rue des Martyrs, F-38 054 Grenoble Cedex, France
[2] Laboratoire d'Etude des Microstructures, ONERA-CNRS, BP 72, F-92322 Châtillon Cedex, France
[3] CEA-CNRS group 'Nanophysique et Semiconducteurs', Institut Néel/CNRS-Université J Fourier and CEA Grenoble, 25 rue des Martyrs, F-38 054 Grenoble Cedex, France
[4] Laboratoire de Physique des Solides, CNRS UMR8502, Université Paris-Sud XI, Bâtiment 510, F-91405 Orsay, France

E-mail: bruno.daudin@cea.fr

Received 22 February 2013, in final form 22 May 2013
Published 2 July 2013
Online at stacks.iop.org/Nano/24/305703

Abstract
The optical properties of single AlGaN nanowires grown by plasma-assisted molecular beam epitaxy have been studied by nanocathodoluminescence. Optical emission was found to be position-dependent and to occur in a wide wavelength range, a feature which has been assigned to a composition gradient along the nanowire growth axis, superimposed on local composition fluctuations at the nanometer scale. This behavior is associated with the growth mode of such AlGaN nanowires, which is governed by kinetics, leading to the successive formation of (i) a zone with strong local composition fluctuations followed by (ii) a zone with a marked composition gradient and, eventually, (iii) a zone corresponding to a steady state regime and the formation of a homogeneous alloy.

(Some figures may appear in colour only in the online journal)

1. Introduction

The current attractiveness of nitride nanowires from both an academic and practical point of view partly comes from their crystalline quality, namely the absence of extended defects such as dislocations, which still limit the performance of devices in the case of bidimensional layers. This is particularly true in the case of ultraviolet (UV) emission, making AlGaN NWs promising candidates for the realization of innovative UV light emitting diodes (LEDs) [1].

In the case of visible LEDs, the high internal efficiency is attributed to a marked carrier localization in the InGaN quantum wells (QWs) forming the active region. Although the underlying reasons for this behavior are still controversial, it has to be mentioned that the large bowing parameter value of InGaN is indicative of a significant alloy disorder [2]. By contrast, a reduced carrier localization has been reported in AlGaN that has been assigned to the absence of marked compositional inhomogeneities, consistent with a smaller bowing parameter than for InGaN alloys [3]. However, this statement has to be seriously modified due to the large dispersion of bowing parameter values observed in the literature, emphasizing the importance of the growth technique and growth parameters [4].

In addition, it has been shown that AlGaN layers show significant in-plane phase separation and weak phase separation along the growth direction [5]. These features have been correlated to structural defects such as dislocations, grain boundaries or atomic steps, leading to compositional fluctuations and, concomitantly, to fluctuations at the micrometer scale in the AlGaN emission wavelength [6].

By contrast, the absence of extended crystallographic defects in NWs and the easy strain relaxation associated with their large aspect ratio should lead to the formation of a homogeneous alloy. However, it has been recently shown that the nucleation kinetics of AlGaN NWs crucially governs their composition, eventually leading to marked compositional fluctuations which depend on the growth temperature [7]. Microphotoluminescence (microPL) experiments have also revealed the presence of localization centers in such AlGaN NWs, likely associated with compositional fluctuations, which were found to result in a reduced quenching of the emission between 10 K and room temperature.

The goal of the present work is to get further insight into the luminescence properties of AlGaN NWs at the nanometric scale. For that purpose, nanocathodoluminescence (nanoCL) experiments have been performed on single AlGaN NWs. It will be shown that carrier localization at the nanometric scale indeed dominates the optical properties of the lower part of the AlGaN NWs, which have being assigned to the formation of nanometric AlGaN clusters of fluctuating composition in the nucleation regime. Next, in the steady state growth regime, nanoCL results are consistent with the formation of a more homogeneous AlGaN alloy, exhibiting a long-range composition gradient along the growth axis.

2. Experimental results

AlGaN NWs used here were grown on a basis of GaN NWs elaborated by plasma-assisted molecular beam epitaxy (PA-MBE) on a Si(111) substrate [8]. After being deoxidized in HF at 10% and introduced in the growth chamber, the substrate was outgassed until the appearance of the 7×7 Si(111) surface reconstruction. The reproducibility of the substrate temperature was ensured by measuring the Ga desorption time following the exposure of the surface to a Ga flux, using the method reported in [9]. GaN NW growth was performed using a N flux of 0.3 ML s^{-1}. The Ga/N ratio and Ga desorption time were set at 1/2 and 6.5 s (approximately 820 °C) respectively. The length and diameter of the resulting GaN bases were 250 nm and 15 nm, respectively.

After completion of the GaN base and without growth interruption, the Al shutter was next opened to start the growth of $Al_xGa_{1-x}N$. The Al/N ratio was set at 1/4. In order to promote homogeneous growth the substrate was continuously rotated. For the study of the optical properties of single AlGaN NWs reported here, we focused on one sample containing around 30% of Al on average. It should be noted that the GaN base growth temperature was chosen high enough to ensure a density of NWs low enough to facilitate their dispersion [9]. Then, for growth of the AlGaN section, the temperature was decreased by 5 °C to keep the AlGaN growth temperature identical to that used in [7]. This procedure resulted in the formation of a 2D layer at the NW base but did not affect the properties of the dispersed NWs.

NanoCL spectral-imaging experiments have been performed as described in [10]. Briefly, a HB 501 VG STEM fitted with a high-throughput CL system is used to form a 60 keV electron beam on the area of interest.

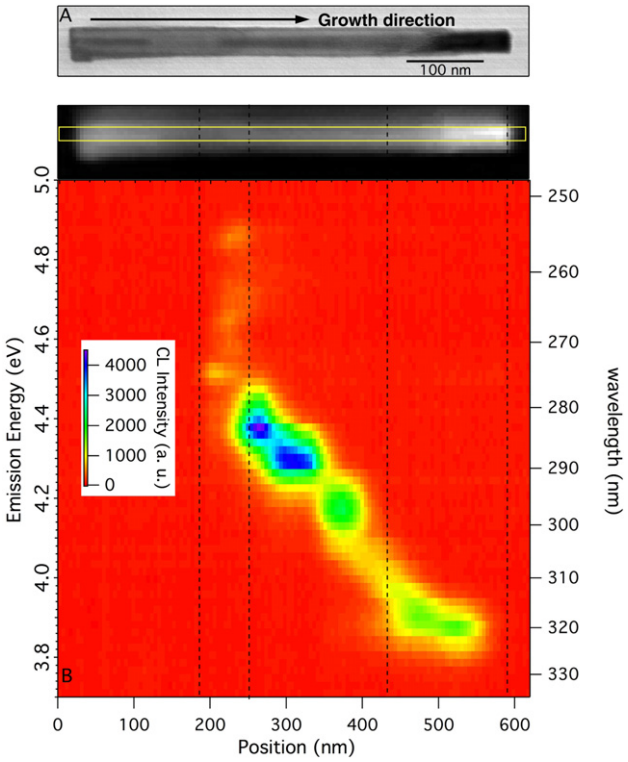

Figure 1. Cathodoluminescence spectral-imaging of a nanowire. (A) Bright-field image of the nanowire. Ga-rich region appear darker. (B) Excerpt from a spectral-image. Top: online ADF image of the nanowire (Ga-rich region appears bright). Bottom: line of spectra along the wire axis represented as a 2D map (energy versus position along the wire). Spectra have been integrated along the perpendicular direction in the range shown by the height of the rectangular region of interest in the ADF. Dotted lines are a guide to the eye to indicate the three regions discussed in the body of the text.

Typical currents for these experiments were 800 pA and the probe size was around 1 nm. The spectral resolution was set to about 1 nm. The sample was cooled down to 150 K. In the spectral-imaging mode, the beam was scanned with a constant increment over the sample of interest. At each point of the scan, both structural (annular dark-field, ADF, and bright-field, BF) and spectroscopic information were recorded. Thus, at the end of the scan, images and spectral-images (images with one spectrum per point) could be reconstructed, allowing one to perform a pixel by pixel correlation. Typical increments and dwell times were 4.9 nm and 5 ms.

Figure 1 shows the nanoCL results corresponding to a representative NW. On the BF image in (figure 1(A)), one notes the presence of the GaN base, identified as a dark zone surrounded by a lighter zone corresponding to the growth of an AlN shell. The presence of this AlN shell has been discussed in a previous paper [7]: it was found to result from the low diffusion of Al compared to Ga. In figure 1(B) is shown a representative data set extracted from a spectral image. On the top is shown the ADF image (where bright contrast corresponds now to Ga-rich areas). In correspondence, the nanoCL map below was built using a series of spectra taken along the nanowire axis and integrated

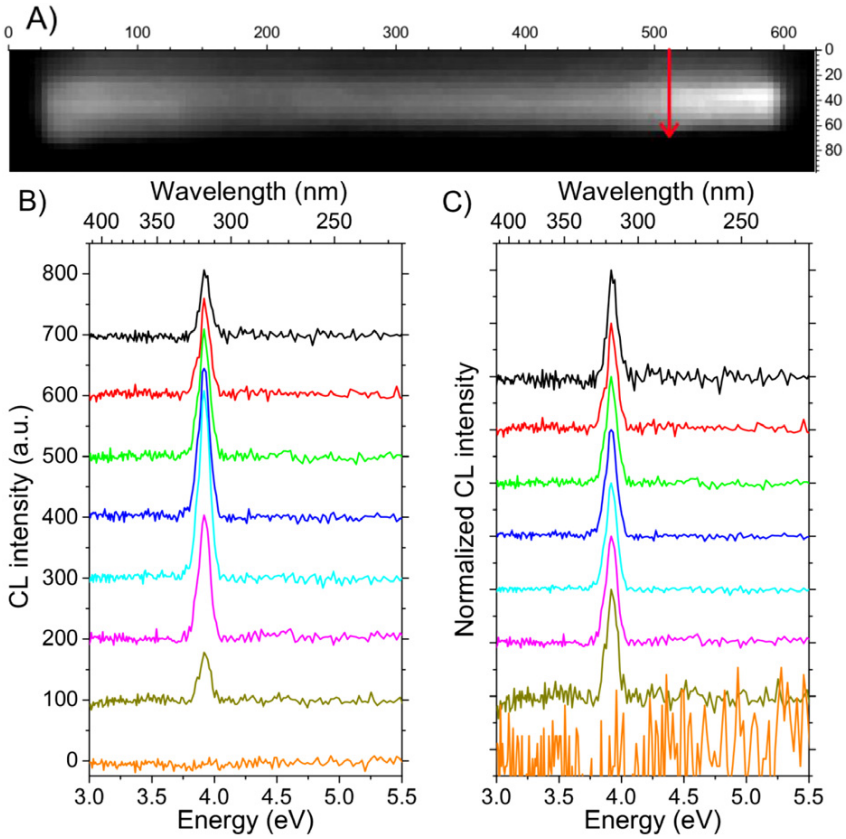

Figure 2. Spectra recorded along the radius at the top of the wire, in the region of the steady state growth regime, as marked by the arrow in the online ADF image in (A): (B) raw data; (C) normalized. The spectra are taken every 10 nm.

over a few pixels in the radial direction (see yellow box on the ADF image). Three regimes can be identified: (i) in the upper 150 nm of the NW (right part of figure 1), the nanoCL peaks at about 3.8–3.9 eV, with no emission at the tip, while (ii) in the 260 nm long section below, a progressive blue shift of the nanoCL peak is observed, associated with a marked decrease in intensity and an increase in peak numbers in the last 60 nm of this section. Finally, (iii) no luminescence was observed in the last 60 nm between the bottom part of the AlGaN section and the top of the GaN base.

Now turning to a more detailed study of the different regions identified above, figure 2 shows the radial evolution of nanoCL in the top section, which was found to be axially homogeneous (the scanning step was 2 pixels, i.e. about 10 nm) with a CL energy peak at 3.9 eV exhibiting a full width at half maximum (FWHM) of about 100 meV. Note that such a CL energy corresponds to an Al content of about 25%, assuming the generally accepted value of 1 eV for the bowing parameter of AlGaN alloy [11] and a low Stokes shift (in accordance to the analysis done in [7]). This is consistent with the nominal Ga/Al flux ratio of 30% used during the growth.

Two similar radial scans have been performed in the zone exhibiting an axial gradient in AlGaN composition, namely at a distance of 205 and 300 nm below the top of the NW, and are shown in figures 3 and 4, respectively. The CL energy is peaked at 4.2 eV (205 nm below the NW top) and at 4.4 eV (300 nm below the NW top). In both cases the FWHM is about 250 meV, significantly larger than in the upper region of the NW and consistent with a larger alloy disorder in this region of the NW. However, limited variations of either the peak energy or FWHM are observed along the radius of the NW, as an indication of radial homogeneity, opposed to the marked composition gradient along the growth axis in this region.

Finally CL spectra recorded in the bottom of the composition gradient region, 375 nm below the top, are shown in figure 5. CL peaks recorded in this region are spanned in an energy window of about 750 meV and exhibit a well marked structure, indicative of strong composition fluctuations. Such fluctuations are localized along the axis and perpendicular to it in regions of the order of about 20–30 nm, as shown in figure 5. The corresponding spectra exhibit a marked variability in both intensity and wavelength emission, as further evidence of a composition fluctuation along both the diameter and the growth axis in this region, in contrast with the situation reported in figures 3 and 4. However, it has to be noted that only a few peaks are observed, as a clue that only a few localization centers are present.

In order to ensure that the results reported above are representative of the NW population studied in the present work, a statistical analysis was further performed on a set of ten NWs. The results are reported in figure 6. First, in figure 6(A), both the CL energy peak and FWHM in the upper part of the ten NWs are reported. The mean CL energy

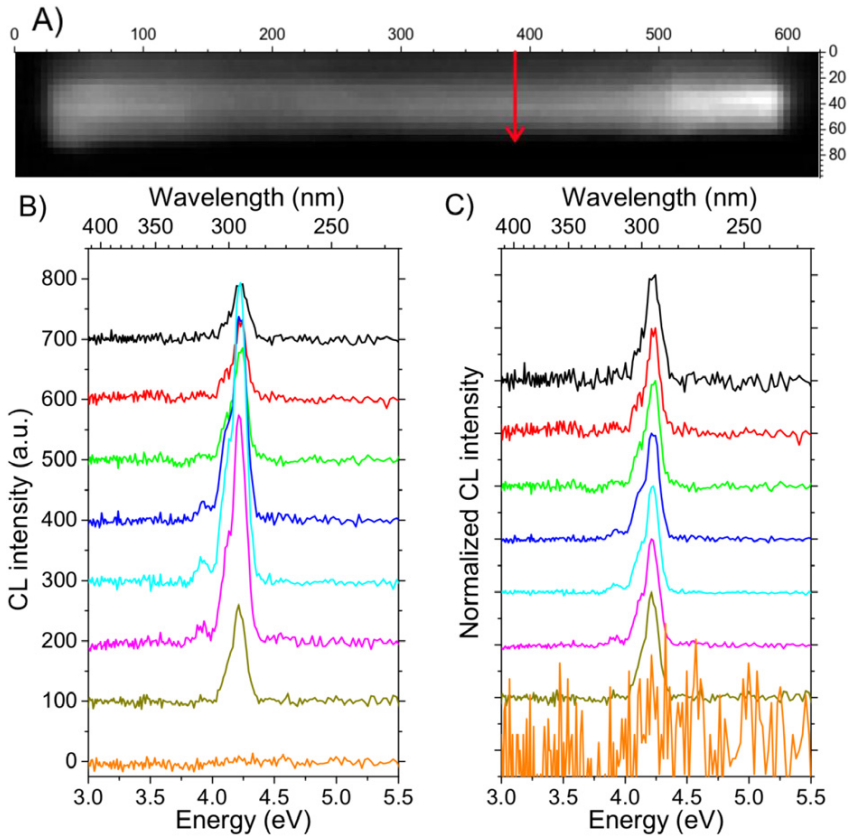

Figure 3. Spectra recorded along the radius 205 nm below the wire top, as marked by the arrow in the online ADF image in (A): (B) raw data; (C) normalized. The spectra are taken every 10 nm.

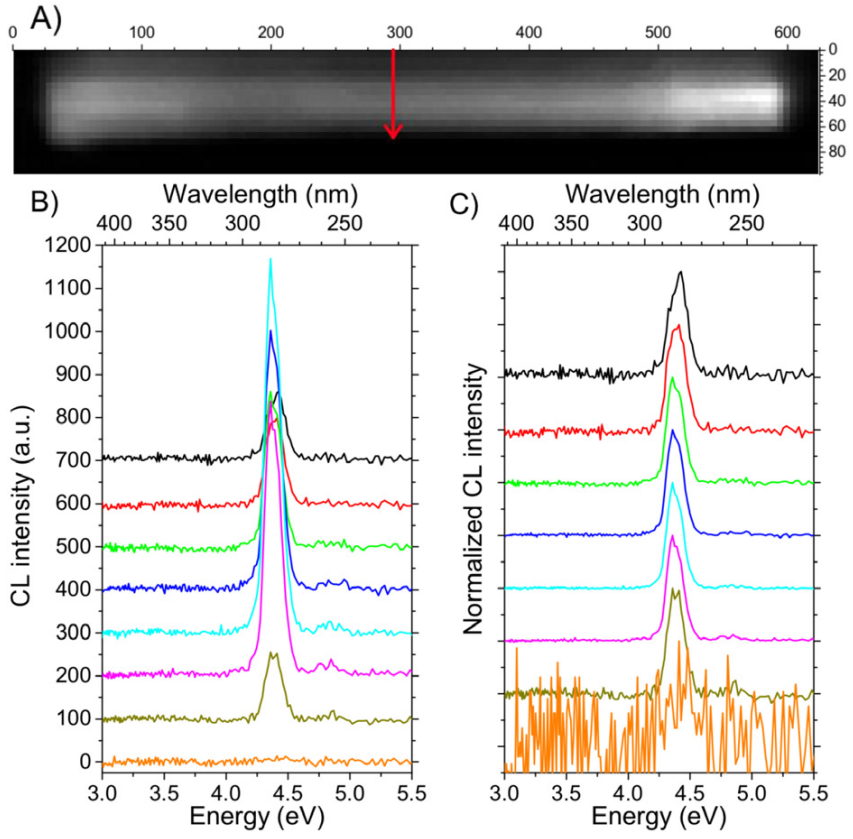

Figure 4. Spectra recorded along the radius 300 nm below the wire top, as marked by the arrow in the online ADF image in (A): (B) raw data; (C) normalized. The spectra are taken every 10 nm.

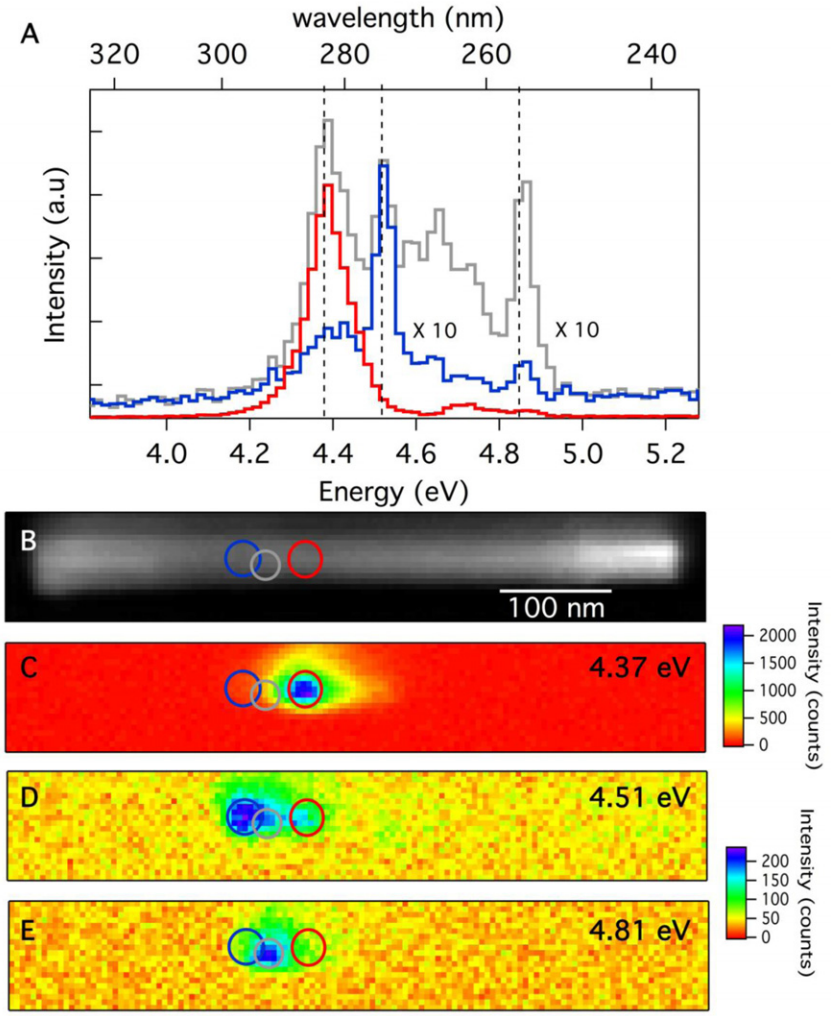

Figure 5. Localization of the CL signal in the nucleation region (A) spectra extracted from regions indicated by the circles in the ADF image shown in (B); (C)–(E) maps of the intensity integrated around one of the main peaks (energy indicated). Although each peak may appear in the three spectra, their intensities are clearly centered in different regions of the nanowire.

peak is found to be about 3.9 eV, for a FWHM spanning between 70 and 120 meV. In figures 6(B) and (C), the energy peaks recorded at a distance of 190 and 375 nm, respectively, below the NW top are reported. In both regions, and for each NW, several peaks are identified. Significantly, the values corresponding to the NW studied above in detail are comprised in the energy range defined by the ensemble of the ten NWs statistically analyzed, as a clear indication of its representativeness with respect to the population of NWs under investigation.

3. Discussion and conclusion

Based on the above nanoCL results, the following scenario can be proposed for the growth of AlGaN NWs: after the completion of a few hundred nm long GaN NW base, the simultaneous exposition of the surface to Ga, Al and N fluxes actually results in the growth of pure AlN on top of the base. This behavior is assigned to the dominant role of kinetics, making the nucleation of pure AlN far more probable than the nucleation of GaN [7] in spite of the epitaxial constraint resulting from the in-plane lattice mismatch between AlN and GaN. Actually, in the growth conditions of the present work, the desorption probability of Ga adatoms is expected to be far larger than that of Al, making the nucleation of GaN islands on top of the base less favorable in competition with AlN nucleus formation. Once the first layers of AlN are formed, the further nucleation of GaN nuclei is even less favorable, due to the lattice mismatch with respect to AlN. As the desorption rate of Ga is not infinite, this situation leads to the progressive accumulation of Ga adatoms on the surface of the growing AlN NW section. After a time depending on Al and Ga flux as well as on growth temperature, the Ga adatom density turns out to be high enough to make the nucleation of GaN nuclei as probable as the nucleation of AlN ones. Following the formation of these AlN and GaN nuclei on the surface, the subsequent statistical incorporation of Al or Ga adatoms is expected to lead to a wide variability of composition at the nm scale, a feature which is tentatively assigned to the onset of the

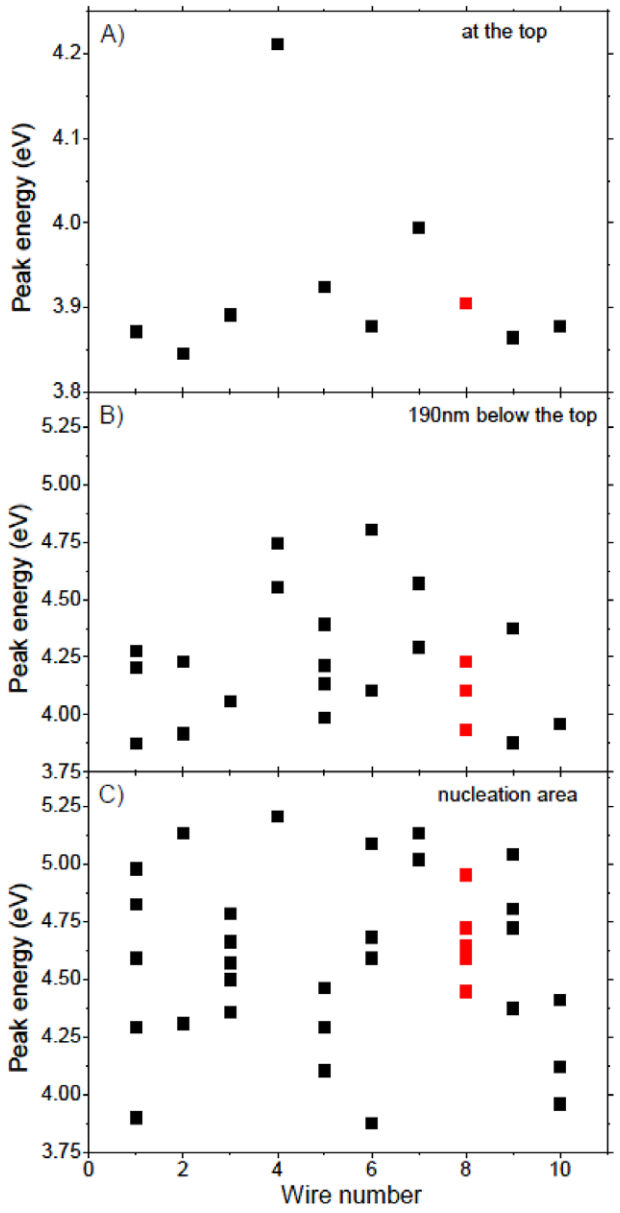

Figure 6. Statistical analysis on ten nanowires taken on the same TEM grid. (A) Energy peak maxima of the CL spectra registered at the top of the ten wires. (B) Energy peak maxima on the spectra registered 190 nm below the wire top. (C) Energy peak maxima on the spectra registered in the region of strong localizations. For all of them, the analyzed wire is in red.

growth of the region where various composition/CL emission lines are observed.

Once the formation of the AlGaN NW section is triggered, the composition gradient observed is assigned to the progressive strain relaxation, making the incorporation of Ga in AlGaN progressively easier. Eventually, once the steady state regime is reached, the upper section of the AlGaN NW exhibits a constant composition, corresponding to the nominal ratio of Ga/Al metal flux, as evidence that this regime corresponds to the statistical incorporation of Al and Ga. It is worth mentioning that such a scenario is consistent with results previously reported for an assembly of NWs [7] and confirms, at the scale of individual NWs, the predominance of kinetics in the growth process.

The contrast in the CL images of the single NWs under study is an indication of the reduced carrier diffusion length in AlGaN. Indeed, it has been previously estimated that the carrier diffusion length in AlGaN at room temperature was about 7.5 nm [12]. This value, corresponding to about 2 pixels in the CL images, can be safely adopted in the case of the present experiments performed at 150 K as further evidence that the CL energy dispersion actually reflects composition fluctuations at the nm scale. Interestingly, the CL signal in the AlGaN nucleation region (figure 5) consists of several peaks, sharper than the peaks corresponding to the steady state region in figure 2. The FWHM of CL peaks in the steady state regime (about 125 meV) is comparable to the results observed in the case of 2D layers and can be assigned to alloy disorder. By contrast, the sharper lines in the nucleation region, which can be fitted to be around 40 meV for some of them, are a clue of significant carrier localization at the nm scale in this region. These features further support the growth model described above, suggesting that random incorporation of Ga and Al adatoms in nuclei may actually result in the formation of marked potential sinks governing the optical behavior of AlGaN alloy in this region.

In conclusion, the nanoCL results presented here allow one to evidence the presence of carrier localization centers in AlGaN NWs, associated with the prominent role of kinetics in the growth of these nanostructures. As a result, three regimes have been observed in the AlGaN NW, namely a nucleation zone exhibiting composition fluctuations in the nm range, a zone exhibiting a composition gradient associated with both nucleation kinetics and progressive strain relaxation along the growth axis, eventually followed by a zone where the AlGaN composition reflects the nominal Ga/Al flux ratio used during the growth. The understanding of the AlGaN NW growth mode at the scale of single NWs supports results obtained for a large collection of wires and potentially provides a way to grow AlGaN NWs in the whole range of composition.

Acknowledgments

We acknowledge Y Curé for help during operation of the MBE machine. The authors acknowledge financial support from the French CNRS (FR3507) and CEA METSA network. The research leading to these results has received funding from the European Union Seventh Framework Programme under Grant Agreement 312483—ESTEEM2 (Integrated Infrastructure Initiative—I3).

References

[1] Sekiguchi H, Kishino K and Kikuchi A 2010 *Electron. Lett.* **44** 151
[2] McCluskey M D, Van de Walle C G, Romano L T, Krusor B S and Johnson N M 2003 *J. Appl. Phys.* **93** 4340
[3] Steude G, Meyer B K, Göldner A, Hoffmann A, Bertram F, Christen J, Amano H and Akasaki I 1999 *Appl. Phys. Lett.* **74** 2456

[4] Yun F, Reshchikov M A, He L, King T, Morkoç H, Novak S W and Wei L 2002 *J. Appl. Phys.* **92** 4837
[5] Sun Q, Huang H, Wang W, Chen J, Jin R Q, Zhang S M, Yang H, Jiang D S, Jahn U and Ploog K H 2005 *Appl. Phys. Lett.* **87** 121914
[6] Pinos A, Marcinkevičius S, Yang J, Nilenko Y, Shatalov M, Gaska R and Shur M S 2009 *Appl. Phys. Lett.* **95** 181914
[7] Pierret A, Bougerol C, Murcia-Mascaros S, Cros A, Renevier H, Gayral B and Daudin B 2013 *Nanotechnology* **24** 115704
[8] Mata R, Hestroffer K, Budagosky J, Cros A, Bougerol C, Renevier H and Daudin B 2011 *J. Cryst. Growth* **334** 177
[9] Landré O, Songmuang R, Renard J, Bellet-Amalric E, Renevier H and Daudin B 2008 *Appl. Phys. Lett.* **93** 183109
[10] Zagonel L F *et al* 2011 *Nano Lett.* **11** 568
[11] Teofilov N, Thonke K, Sauer R, Kirste L, Ebling D G and Benz K W 2002 *Diamond Relat. Mater.* **11** 892
[12] Barjon J, Brault J, Daudin B, Jalabert D and Sieber B 2003 *J. Appl. Phys.* **94** 2755